ARTICLE IN PRESS

Journal of Biomechanics ∎ (∎∎∎∎) ∎∎∎–∎∎∎

Contents lists available at ScienceDirect

Journal of Biomechanics

journal homepage: www.elsevier.com/locate/jbiomech
www.JBiomech.com

The effect of static muscle forces on the fracture strength of the intact distal radius *in vitro* in response to simulated forward fall impacts

Jacob M. Reeves, Timothy A. Burkhart, Cynthia E. Dunning *

Jack McBain Biomechanical Testing Laboratory Department of Mechanical and Materials Engineering, Western University, 1151 Richmond St, London, ON N6A 5B9, Canada

A R T I C L E I N F O

Article history:
Accepted 17 May 2014

Keywords:
Distal radius
Fracture
Muscle force
Impact
Trauma

A B S T R A C T

The distal radius fracture (DRF) is a particularly dominant injury of the wrist, commonly resulting from a forward fall on an outstretched hand. In an attempt to reduce the prevalence, costs, and potential long-term pain/deformities associated with this injury, *in vivo* and *in vitro* investigations have sought to classify the kinematics and kinetics of DRFs. *In vivo* forward fall work has identified a preparatory muscle contraction that occurs in the upper extremity prior to peak impact force. The present investigation constitutes the first attempt to systematically determine the effect of static muscle forces on the fracture threshold of the distal radius *in vitro*. Paired human cadaveric forearm specimens were divided into two groups, one that had no muscle forces applied (*i.e.*, right arms) and the other that had muscle forces applied to ECU, ECRL, FCU and FCR (*i.e.*, left arms), with magnitudes based on peak muscle forces and *in vivo* lower bound forward fall activation patterns. The specimens were secured in a custom-built pneumatic impact loading device and subjected to incremental impacts at pre-fracture (25 J) and fracture (150 J) levels. Similar fracture forces (6565 (866) N and 8665 (5133) N), impulses (47 (6) Ns and 57 (30) Ns), and energies (152 (38) J and 144 (45) J) were observed for both groups of specimens ($p > 0.05$). Accordingly, it is suggested that, at the magnitudes presently simulated, muscle forces have little effect on the way the distal radius responds to forward fall initiated impact loading.

1. Introduction

Distal radius fractures are among the most prevalent fractures in the body (Shauver et al., 2011; Van Staa et al., 2001) having an incidence rate nearly twice that of hip/femur fractures, and nearly five times that of vertebral/spine fractures (Van Staa et al., 2001). It has been estimated that 39% of wrist fractures in the elderly (> 65 years) occur as a result of a forward fall (Nevitt and Cummings, 1993), and often these injuries result in long term pain and deformity (Altissimi et al., 1986; MacDermid et al., 2003). The financial burden of distal radius fractures is also high, estimated at approximately $2000 USD per incident (Gabriel et al., 2002; Shauver et al., 2011). As a result of the severity and financial costs of distal radius fractures, *in vivo* and *in vitro* investigations have been conducted in an attempt to determine the kinematics and kinetics associated with these injuries with the aim of decreasing their occurrence.

One of the important findings from the *in vivo* fall studies has been the identification of a preparatory muscle response. It was reported that upper extremity muscle activation peaked prior to peak impact force, suggesting that individuals attempt to prepare themselves during fall initiated impacts in an attempt to prevent injury (Burkhart and Andrews, 2013; Dietz et al., 1981). It is thought that muscle force application can lead to improved joint stability (McGill et al., 2003; Santello, 2005), which may reduce the risk of injury. However, muscle force increase can also result in a stiffer segment (Challis and Pain, 2008; Nigg and Liu, 1999; Pain and Challis, 2002; Pain and Challis, 2001), which can act to propagate the impact shock increasing the risk for injury (Burkhart and Andrews 2010). Moreover, these forces are thought to lead to pre-straining across the wrist joint prior to external load application (Duda et al., 1998). It is possible that this could lead to lower ultimate failure stresses of the wrist joint bones prior to the application of external loads.

Despite the identification of a pre-impact muscle response and the ambiguity of its effects on injury, only one known *in vitro* distal radius fracture study has simulated muscle forces in the upper extremity. However, this study failed to document the magnitude of the applied muscle loads, which were only used to position the wrist in extension (McGrady et al., 2001). Therefore, the purpose of the current study was to determine the effect of static forearm muscle forces on the fracture strength of the distal radius following systematically applied impacts representative of forward falls.

* Corresponding author.
E-mail addresses: jakereeves5@gmail.com (J.M. Reeves), tburkhar@uwo.ca (T.A. Burkhart), cdunning@uwo.ca (C.E. Dunning).

http://dx.doi.org/10.1016/j.jbiomech.2014.05.010
0021-9290/

Please cite this article as: Reeves, J.M., et al., The effect of static muscle forces on the fracture strength of the intact distal radius *in vitro* in response to simulated forward fall impacts. Journal of Biomechanics (2014), http://dx.doi.org/10.1016/j.jbiomech.2014.05.010

2. Methods

Using a custom designed pneumatic impact loading apparatus (Fig. 1), 12 paired fresh-frozen cadaveric forearm (disarticulated at the elbow, with an intact wrist joint) specimens from 3 male and 3 female donors (mean (SD) age 63 (11) years, height 171 (13) cm, weight 66 (31) kg) were tested. Each specimen was screened for bone affecting diseases (*e.g.*, osteoporosis) by the specimen procurement agency to ensure that the sample was representative of a healthy population. Further analysis of bone quality was conducted by measuring the apparent density and cross-sectional area of the distal third, distal tenth and ultra distal (*i.e.*, directly subchondral) radius. Both measures were obtained using Mimics CT image processing software (Materialise; Belgium), where apparent density was quantified from the average Houndsfield Unit (HU) at each distance by using a linear HU-density (g/mm^3) relationship derived from scanned water and hydroxyapatite phantoms. In addition, cross-sectional area was determined by matching an ellipse to the radius' axial cross-section at each distance and all measurements were taken from the CT scans of the pre-impacted specimens. The impact apparatus operates by applying acute loads to the specimen *via* a weighted (6.66 kg) ram that is translated down an acceleration tube under the influence of pressurized air. Upon exiting the acceleration tube the ram strikes an impact plate assembly transferring the force through a load cell (6 Degree of Freedom, Denton femur load cell model: 1914A; Denton ATD, Inc. Rochester Hills, MI), and onto the specimen (Fig. 1). The magnitude of the impact velocity and force is user-controlled by adjusting the air pressure in the tube.

Prior to testing the proximal 8–10 cm of soft tissues were removed from the specimens to permit potting, while ensuring that the interosseous membrane remained intact. Specimens were then fixed in full pronation and potted in 5–7 cm of PVC tubing using dental cement (Denstone Golden, Heraeus Dental; South Bend, IN). A laser level was used in combination with a custom potting jig to ensure sagittal (long forearm axis aligned with centered markings on the potting jig) and frontal (wrist in a neutral posture, the long axis of the third phalange aligned with a central marking on the potting jig) plane specimen alignment. During the cementing process, four plastic tubes were aligned with holes in the potting apparatus to allow for the passage of steel muscle tension cables. Once the specimens were potted, longitudinal incisions were made on the mid-dorsal and mid-palmar sides of the forearm, and the tendons of extensor carpi ulnaris (ECU), extensor carpi radialis longus (ECRL), flexor carpi ulnaris (FCU), and flexor carpi radialis (FCR) were isolated from the surrounding musculature and sutured to steel cables using 0.5 mm thread (Spider Wire; Spirit Lake, IA; 100 lb capacity) using a Krackow technique (Krackow et al., 1986), which maintained cable-to-tendon coupling throughout the impact. The selection of these muscles was based on previously collected *in vivo* data (Burkhart and Andrews, 2013). The forearms were then sutured closed to maintain internal moisture. Two incisions were then made on the dorsal aspect of each forearm, just proximal to extensor retinaculum, exposing the ulnar and radial bone surfaces. Here, two 45° strain-gauge rosettes (SGD-3/350-RY53, Omega Environmental; Laval, QC) were applied (using a procedure modified from Staebler et al. (1999) and Austman et al. (2007)) such that the central gauges were visually aligned with the long axis of each respective bone (Fig. 2). The gauges were then insulated using a flexible fast-drying silicone sealant (Alex Fast Dry, DAP; Baltimore; MD). Finally, pilot testing revealed that the phalanges interfered with the base plate of the impact apparatus preventing full range of motion. Therefore, the specimen phalanges were disarticulated at the metacarpal–phalange joint to avoid interference.

The specimens were placed in the impact apparatus' hanging potting mount (Fig. 3) such that the long axis of the forearm was aligned at 75° in the sagittal plane consistent with a forward fall (Burkhart et al., 2012b). A laser level was used (in combination with a vertical marking on the hanging potting mount) to ensure that no rotation was present about the long axis of the forearm. Buttressing the specimen's palmar surface against the secondary impact plate was used to set wrist extension (Fig. 4). To permit secondary impact plate motion tracking, a custom white marker (approximately 1 cm diameter) with a black border was placed on the plate, in-line with the load cell's *z*-axis. Three additional markers were also placed on the visible side of the specimen, one on the radial/ulnar diaphysis (10 cm proximal to the wrist), one at the radiocarpal (wrist) joint (determined through repeated flexion extension), and one at the distal end of the visible metacarpal (Fig. 4). Finally, to simulate an appropriate effective mass acting through the forearm (Chiu and Robinovitch, 1998), each specimen was ballasted to 40–50% (determined through pilot testing) of the donor's body mass by securely strapping weights to the potting mount.

Specimens from each pair were divided into one of two groups: muscle force (left arms), no muscle force (right arms). The magnitude of static muscle forces applied to each muscle was established using *in vivo* forward fall muscle activation patterns (Burkhart, 2011; Burkhart and Andrews, 2013), in combination with peak muscle forces (Holzbaur et al., 2005). Therefore, the resulting force targets were 19, 61, 9, and 5 N for ECU, ECRL, FCU and FCR, respectively. The force in each muscle was set by adjusting the position of a line tightener (C78990V; Ben-Mor Cables Inc. Calgary, AB) buttressed against the back of the potting mount, and measured using a digital tension scale (78-0069-4; Matzuo America; South Sioux City, NE); where tension was applied until the line tightener began to lift off the back of the potting mount. The force in each musclulotendinous unit was measured three times, with impact immediately following the third set of measurements.

Each specimen was subjected to a velocity controlled (measured with two LED sensors Burkhart and Andrews, 2013) pre-fracture impact of 25 J (kinetic energy), and a fracture (defined as a break in the continuity of either the radius or ulna) impact of 150 J (kinetic energy; targets determined through incremental pilot testing). In the event that a specimen did not fracture at 150 J impact, loading was

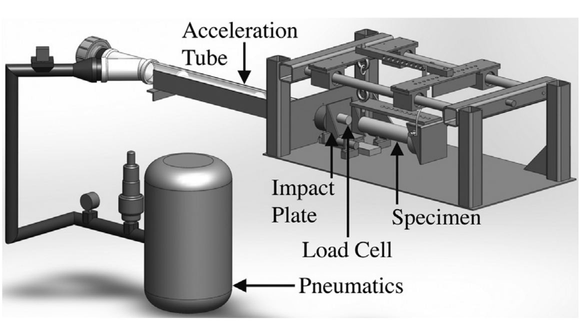

Fig. 1. Schematic representation of the impact apparatus used to apply impact loading. Highlighted is the pneumatic system, acceleration tube, and impact chamber where the specimen is suspended.

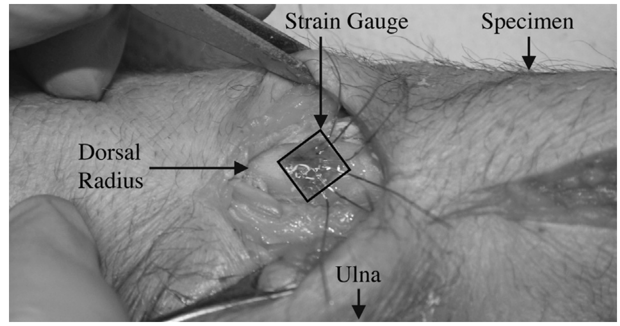

Fig. 2. Dorsal placement of the strain gauges such that the axial gauge was aligned with the long-axis of the bone (left arm shown).

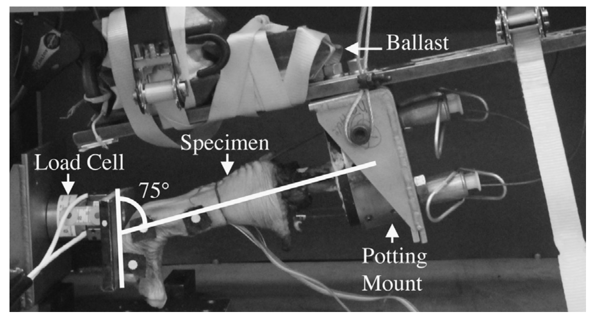

Fig. 3. Specimen orientation as suspended in the impactor at 75° in the sagittal plane, where the palm is buttressed against the load cell's secondary impact plate.

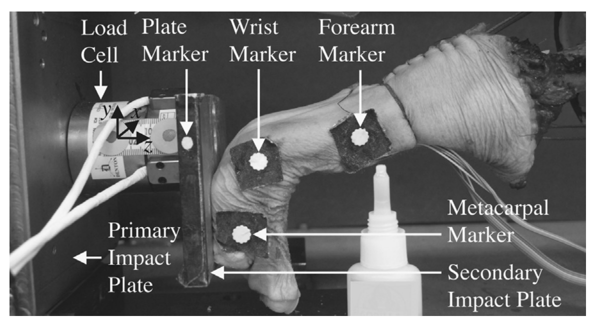

Fig. 4. Specimen and secondary impact plate motion tracking marker orientations that permit determination of the pre-impact wrist extension angle and marker velocities. Also shown is the load cell coordinate system orientation.